Compression mode resonances in ^{90}Zr

D. H. Youngblood, Y.-W. Lui, B. John,* Y. Tokimoto, H. L. Clark, and X. Chen
Cyclotron Institute, Texas A&M University, College Station, Texas 77843, USA
(Received 18 February 2004; published 20 May 2004)

The giant resonance region from 10 MeV$<E_x<$55 MeV in ^{90}Zr has been studied with inelastic scattering of 240 MeV α particles at small angles including 0°. The isoscalar monopole resonance was found to contain 100±12% of the $E0$ energy weighted sum rule with a centroid of $(17.81+0.32-0.20)$ MeV. Eighty one percent of the isoscalar $E1$ energy weighted sum rule was located in two peaks having $E_x=(17.1\pm0.4)$ and (26.7 ± 0.5) MeV, $\Gamma=(5.4\pm0.3)$ and (8.8 ± 1.0) MeV, and containing 13±3% and 70±10%, respectively, of the $E1$ energy weighted sum rule.

DOI: 10.1103/PhysRevC.69.054312 PACS number(s): 24.30.Cz, 25.55.Ci, 27.60.+j

I. INTRODUCTION

The locations of the isoscalar giant monopole resonance (GMR) and giant dipole resonances (ISGDR) are important because their energies can be directly related to the nuclear compressibility and from this the compressibility of nuclear matter ($K_{\rm NM}$) can be obtained [1,2]. We have previously reported measurements of $E0$ and $E1$ giant resonance strength [3,4] in ^{90}Zr using small angle inelastic α scattering at 240 MeV. The $E0$ [3] strength distribution in ^{90}Zr was found to extend up to $E_x\sim25$ MeV rather than being a Guassian centered at about 16 MeV as had been previously reported. This changed the centroid of the strength significantly and brought the value of $K_{\rm NM}$ obtained from the energy of the ^{90}Zr GMR in agreement with that obtained from the GMR energies in ^{116}Sn, ^{144}Sm, and ^{208}Pb. We have also reported [4] observation of the ISGDR in ^{90}Zr (as well as in ^{116}Sn and ^{208}Pb), but with the strength split into two components, qualitatively consistent with the predictions of Colò *et al.* [5] and Vretenar *et al.* [6] who argue that the upper component is the compression mode. However the energies we obtained for the two components differed considerably from the predictions. Furthermore, only 40% of the $E1$ strength was identified in that work (though it was erroneously reported in Ref. [4] that a total of 122% of the $E1$ strength had been identified—see discussion below). We have developed a new detector system that measures both vertical and horizontal scattering angles which significantly improves measurements made with the spectrometer at 0°. Therefore we have studied ^{90}Zr again with this much improved experimental system.

II. EXPERIMENTAL TECHNIQUE AND DATA ANALYSIS

Beams of 240 MeV α particles from the Texas A&M K500 superconducting cyclotron bombarded a self-supporting Zr foil 3.9 mg/cm^2 thick, enriched to 98% in ^{90}Zr, located in the target chamber of the multipole-dipole-multipole spectrometer [7]. The useful horizontal and vertical acceptances of the spectrometer were measured by placing appropriate slits at the entrance to the spectrometer and found to be approximately 5°, in agreement with calculations using RAYTRACE [8]. A slit at the entrance to the spectrometer (approximately 5° horizontally and 6° vertically) was used to block particles that would otherwise scatter from internal components of the spectrometer.

The focal plane detector (approximately 50 cm deep and 60 cm long) consisted of resistive wire detectors used to measure position and angle in the scattering plane (described in Ref. [9]) and two pairs of drift chambers [10] located before and after the horizontal detector which measure the position and angle normal to the scattering plane. The "transparency" of the detector system (percentage of uniformly distributed particles that pass through without hitting any wires) was calculated to be approximately 90%. A plastic scintillator at the exit provided a timing and total energy signal. In the scattering plane, position resolution of approximately 0.9 mm and scattering angle resolution of about 0.09° were obtained. The out-of-plane scattering angle resolution is ρ dependent due to the optical properties of the spectrometer (the angle resolution of the detector is independent of position) and was approximately 0.3° in the giant resonance region improving to better than 0.1° at $E_x\sim50$ MeV. The focal plane detector covered from $E_x\sim9$ MeV to $E_x\sim56$ to 64 MeV, depending on scattering angle. Using a combination of energy loss measured in ion chambers placed between the resistive wires and total energy measured in the scintillator, α particles could be distinguished from other ions (primarily deuterons).

At $\theta_{\rm spec}=0°$, runs with an empty target frame had an α-particle rate approximately 1/2000 of that with a target in place and α particles were uniformly distributed in the spectrum. Cross sections were obtained from the charge collected, target thickness, dead time, and known solid angle. The target thickness was measured by weighing and checked by measuring the energy loss of the 240 MeV α beam in each target. The cumulative uncertainties in target thickness, solid angle, etc., result in about a ±10% uncertainty in absolute cross sections. ^{24}Mg spectra were taken before and after each run with each target and the (13.85 ± 0.02) MeV $L=0$ state [11] was used as a check on the calibration in the giant resonance region.

*Present address: Nuclear Physics Division, Bhabha Atomic Research Center, Mumbai-400085, India.

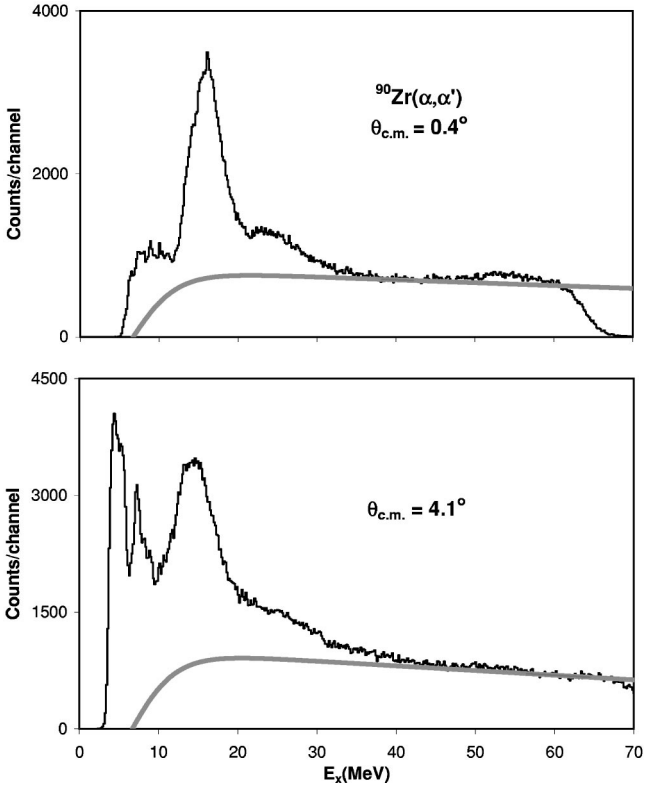

FIG. 1. Inelastic α spectra obtained at two angles for ^{90}Zr. The thick gray lines show the continuum chosen for the analysis.

Sample spectra obtained are shown in Fig. 1. The giant resonance peak can be seen extending up past $E_x = 30$ MeV. The spectrum was divided into a peak and a continuum where the continuum was assumed to have the shape of a straight line at high excitation joining onto a fermi shape at low excitation to model particle threshold effects [12]. Samples of the continua used are shown in Fig. 1.

III. MULTIPOLE ANALYSIS

The multipole components of the giant resonance peak were obtained [12] by dividing the peak into multiple regions (bins) by excitation energy and then comparing the angular distributions obtained for each of these bins to distorted wave Born approximation (DWBA) calculations. The uncertainty in the strength of each multipole due to the fitting process was determined for each multipole by incrementing (or decrementing) that strength, then adjusting the strengths of the other multipoles to minimize total χ^2. This continued until the new χ^2 was 1 unit larger than the total χ^2 obtained for the best fit.

Optical parameters for the calculations were determined from elastic scattering [12] and are given in Table I along with Fermi parameters used for the density distribution of the nuclear ground state. Single folding density dependent DWBA calculations (as described in Refs. [9,13]) were carried out with the code PTOLEMY [14]. The transition densities, sum rules, and DWBA calculations were discussed thoroughly in Ref. [15] and, except for the isoscalar dipole, the same expressions and techniques were used in this work. The transition density for inelastic α particle excitation of the ISGDR given by Harakeh and Dieperink [16] (and described in Ref. [15]) is for only one magnetic substate, so that the transition density given in Ref. [15] must be multiplied by the square root of 3 in the DWBA calculation.

TABLE I. Optical and Fermi parameters used in DWBA calculations.

V (MeV)	V_i (MeV)	r_i (fm)	a_i (fm)	c (fm)	a (fm)
40.2	40.9	0.786	1.242	4.901	0.515

A sample of the angular distributions obtained for the giant resonance (GR) peak and the continuum are shown in Fig. 2. Fits to the angular distributions were carried out with a sum of isoscalar 0^+, 1^-, 2^+, 3^-, and 4^+ strengths. The isovector giant dipole resonance (IVGDR) contributions were calculated from the known distribution [17] and held fixed in the fits. Sample fits obtained, along with the individual components of the fits, are shown superimposed on the data in

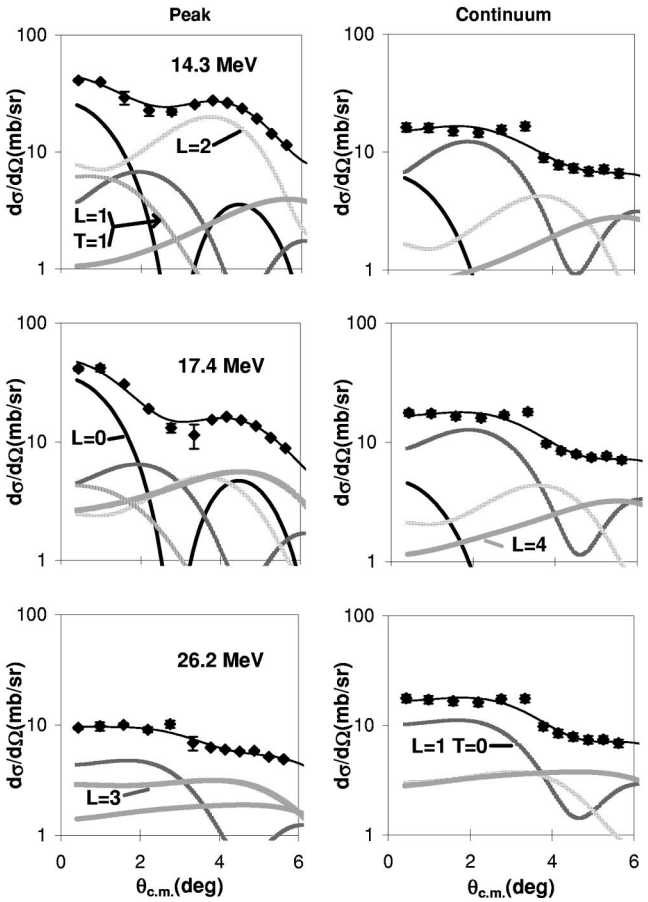

FIG. 2. The angular distributions of the ^{90}Zr cross sections for an 800 keV wide bin centered at the excitation energy indicated on the figure (in MeV) for inelastic α scattering for three excitation ranges of the GR peak and the continuum. The lines through the data points indicate the multipole fits. Contributions of each multipole are shown. The statistical errors are smaller than the data points.

Fig. 2. The continuum distributions are similar over the entire energy range, whereas the angular distributions of the cross sections for the peak change as the contributions of different multipoles dominate in different energy regions. The effects of variations in continuum choices on the extracted multipole distributions was explored as described in Ref. [18].

The (isoscalar) $E0$, $E1$, $E2$, and $E3$ multipole distributions obtained are shown in Fig. 3 and the energy moments and sum rule strengths obtained are summarized in Table II. Due to the limited angular range of the data, $E4$ strength could not be distinguished from higher multipoles and those results are not included. Several analyses were carried out to assess the effects of different choices of the continuum on the resulting multipole distributions. Analyses were made using continua chosen with several different criteria [e.g., (a) using a slope for the linear part which did not quite match the data at high excitation; (b) lowering the continua so that it was always below the data; (c) changing the low energy cutoff and slope of the continuum; and (d) deliberately altering the continuum slope and/or amplitude at only selected angles]. The strength distributions obtained from these analyses were then averaged, and errors calculated by adding the errors obtained from the multipole fits in quadrature to the standard deviations between the different fits. In general the $E0$ and lower part of the $E2$ distributions were relatively insensitive to the continuum choices while the $E1$ and $E3$ distributions were more dependent on the continuum choices [18]. The $E1$ distribution was also fit with two Guassians and these are also shown in Fig. 3 and the parameters obtained are listed in Table II.

The continuum distributions are fit primarily by $L=1$ and $L=2$ angular distributions, with some small amount $L=0$ at lower excitation and in some cases $L=4$ at higher excitation. This continuum "$E1$" and "$E2$" strength corresponds to many times the EWSR's for each of the nuclei and hence (most of it) cannot be due to inelastic excitation of $E1$ or $E2$ strength in the target nuclei. The possible contributions to the continuum are discussed thoroughly in Ref. [18].

IV. DISCUSSION

The $E0$ distribution shown in Fig. 3 consists of a peak around $E_x=16.9$ MeV with a "tail" extending up past $E_x=25$ MeV containing 100% of the isoscalar $E0$ energy weighted sum rule (EWSR) and has a centroid of $(17.81+0.32-0.20)$ MeV. This GMR distribution is compared to that reported by Youngblood, Lui, and Clark [3] in Fig. 4 and the agreement is excellent. Earlier works identified only the $E0$ strength in the peak. A Hartree-Fock random-phase approximation calculation by Hamamoto *et al.* [19] showed a very similar tail on the GMR peak in ^{90}Zr and this calculation is superimposed on the data in Fig. 5. The values obtained for the centroid (m_1/m_0) and for $(m_1/m_{-1})^{1/2}$ in this work and in Ref. [3] are in excellent agreement.

The $E1$ distribution is separated into at least two peaks and has been fit with two Gaussians (shown in Fig. 3) with centroids of (17.1 ± 0.4) MeV and (26.7 ± 0.5) MeV containing $13\pm3\%$ and $70\pm10\%$ of the isoscalar $E1$ EWSR. The upper component is expected to be the compression mode [5,6] while the structure of the lower component is an open question [5,6]. The only previous report of ISGDR strength in ^{90}Zr was in Ref. [4] where a total of 40% of the $E1$ EWSR

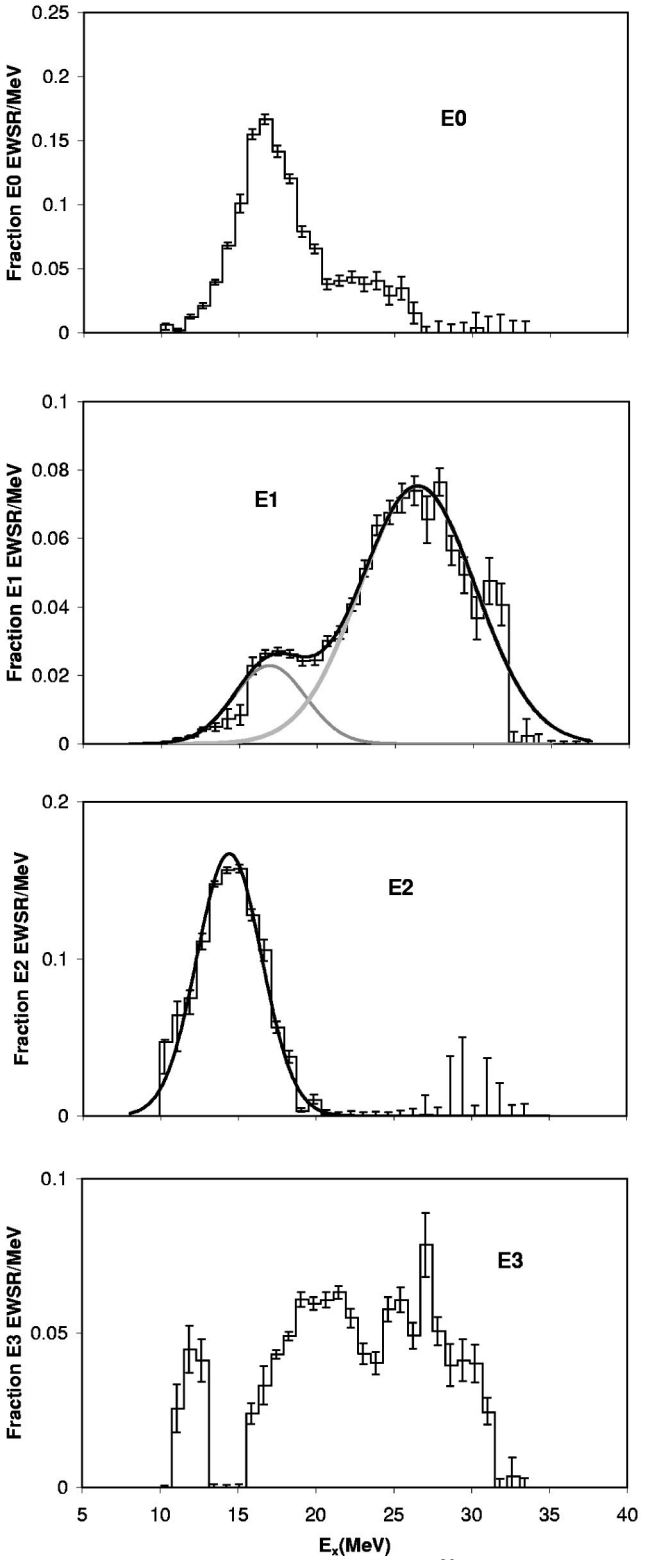

FIG. 3. Strength distributions obtained for ^{90}Zr are shown by the histograms. Error bars represent the uncertainty due to the fitting of the angular distributions and different choices of the continuum as described in the text. The smooth lines show Gaussian fits.

TABLE II. Paramameters obtained for isoscalar multipoles in ^{90}Zr.

	Moments											
	$E0$	− Error	+ Error	$E1$	− Error	+Error	$E2$	− Error	+ Error	$E3$[a]	− Error	+ Error
m_1 (fraction)	1.00	0.12	0.12	0.81	0.10	0.10	0.88	0.08	0.11	0.78	0.15	0.09
m_1/m_0 (MeV)	17.81	0.20	0.32	24.15	0.50	0.60	14.30	0.12	0.40	22.91	0.50	0.70
rms width (MeV)	3.35	0.35	0.60	4.63	0.40	0.70	2.14	0.25	0.45	4.27	0.45	0.60
$(m_3/m_1)^{1/2}$ (MeV)	18.69	0.30	0.65									
$(m_1/m_{-1})^{1/2}$ (MeV)	17.55	0.18	0.25									

	Gaussian fits		
	$E1$ Pk1	$E1$ Pk2	$E2$
Centroid (MeV)	17.1±0.4	26.7±0.5	14.65±0.20
FWHM (MeV)	5.4±0.3	8.8±1.0	4.9±0.2
Fraction EWSR	0.13±0.03	0.70±0.10	0.88±0.09

	$E2$		
	Buenerd *et al.* [21]	Borghols *et al.* [23]	Youngblood *et al.* [22]
Centoid (MeV)	14.05±0.3	14.0±0.4	14.0±0.2
FWHM (MeV)	4.0±0.3	3.0±0.5	3.4±0.2
Fraction EWSR	0.51		0.66±0.17

	HEOR	
	Bertrand *et al.* [28]	Yamagata *et al.* [29]
Centroid (MeV)	27	26.5±1.5
FWHM (MeV)	9±1	
Fraction EWSR	0.18±0.04	0.47±0.20

[a]Moments for HEOR only ($E_x > 15$ MeV).

was identified. It was erroneously reported in Ref. [4] that 122% of the $E1$ EWSR was observed, however the normalization of the $E1$ distributions reported in that work was off by a factor of 3 because the Harakeh and Dieperink [16] sum rule used is for only one magnetic substate. The $E1$ distribution from Ref. [4], renormalized by this factor of 3, is compared to the present work in Fig. 4. While the shapes of the distributions are similar, approximately twice as much strength was observed in the present work. This is in part due to the much better peak to continuum ratio in the 0° data and in part due to the much better coverage of the angle range from 0 to 3° where the isoscalar dipole is strongest. The better peak to continuum ratio is due both to the elimination of events scattered from the top and bottom slits (using the vertical angle measurement) and to the better overall angular resolution since the previous measurement averaged over the vertical opening of the spectrometer. With the vertical measurement and ray tracing we can now bin the events into spectra corresponding to ~0.5° bins from average center of mass angles of 0.4° to 3.3° whereas without the vertical measurement the resulting average over the vertical opening results in 0° data only from average center of mass angles of 1° to 2°. The smallest useful angle obtained from the first $\theta_{\rm spec} > 0°$ angle is $\theta_{\rm c.m.} = 3.1°$.

Piekarewicz [20] has carried out self-consistent calculations of both isoscalar monopole and dipole compressional modes in a relativistic random-phase approximation (RRPA), and the resulting strength distributions using the NLC interaction ($K_{\rm NM} = 224$ MeV) are shown (with an arbitrary normalization) superimposed on our data in Fig. 5. Except for a few hundred keV shift, the calculated GMR distribution is in remarkable agreement with the data over the entire energy range. However the experimental centroid of the upper component of the ISGDR is nearly 5 MeV less than that of the calculated distribution. A portion of this might be attributed to strength not yet located in the experiment as only 81±10% of the isoscalar $E1$ strength was located in the experiment. Colò *et al.* [5] calculated ISGDR distributions in nonrelativistic RPA and their result for ^{90}Zr using the force SGII ($K_{\rm NM} = 215$ MeV) is superimposed on our data in Fig. 6. They identify the peaks above $E_x \sim 22$ MeV as the compression mode, with the lower peaks being of another origin. The center of their compression mode strength lies several MeV above the center of the higher peak, which might be attributed to strength missed experimentally. The lower components are in somewhat better agreement with the data, particularly considering the $E_x \sim 10$ MeV lower cutoff of the data. In heavier nuclei such as ^{144}Sm and ^{208}Pb where 97 +10−20 % and 114+12−25 % of the $E1$ EWSR were observed [18] theoretical calculations which generally reproduce GMR energies show the compression mode ISGDR several MeV above the experimental peaks.

The $E2$ strength is concentrated in an (almost) Gaussian peak centered at 14.65±0.20 MeV containing 88±9% of the isoscalar $E2$ EWSR. Results from three earlier measurements [21–23] of GQR strength in ^{90}Zr are listed in Table II. None of the earlier measurements took into account the (now known) $E0$, $E1$, and $E3$ strength lying above the (then

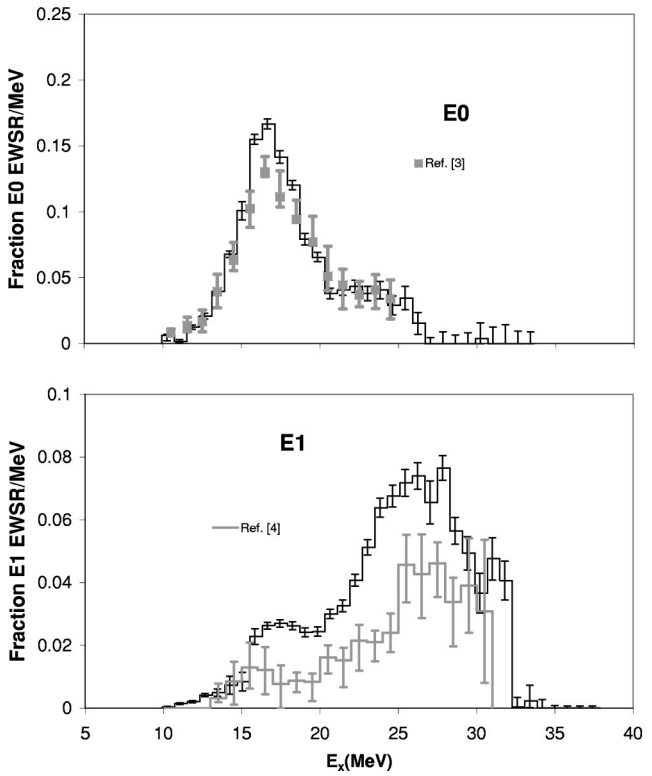

FIG. 4. The $E0$ distribution obtained in this work is compared to that from Ref. [3] in the top panel. The $E1$ distribution obtained in this work is compared to that from Ref. [4] in the bottom panel. The distribution from Ref. [4] has been renormalized as discussed in the text.

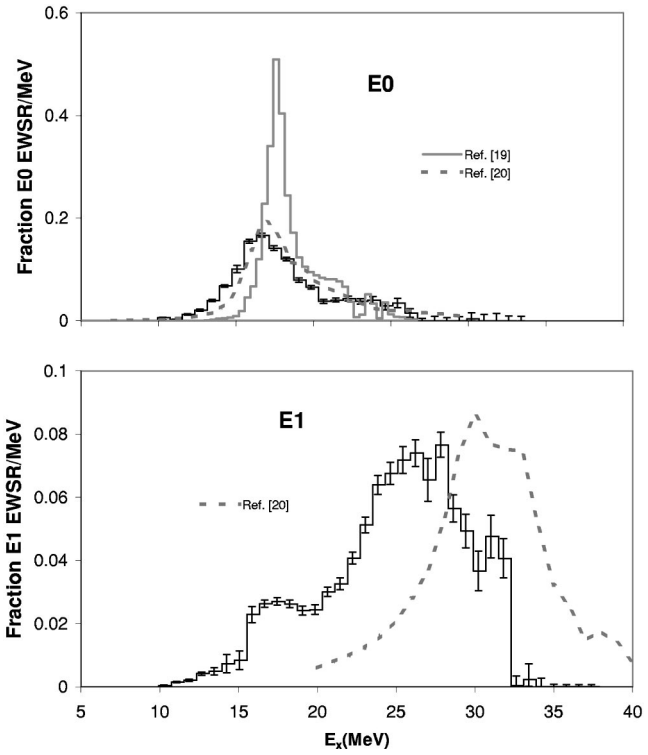

FIG. 5. (Top) Calculations by Hamamoto, Sagawa, and Zhang [19] and by Piekarewicz [20] are compared to the experimental $E0$ strength distribution. (Bottom) Calculations by Piekarewicz [20] are compared to the experimental $E1$ strength distribution.

known) $E2$ and $E0$ peaks, probably resulting in the assumption of an unrealistically high continuum at higher excitation. This would result in lower strengths, lower excitation energies, and smaller widths for the GQR than obtained in the present measurements, all consistent with the values in Table II.

Ma *et al.* [24] have calculated the ISGQR distribution in ^{40}Ca, ^{90}Zr, and ^{208}Pb (as well as ^{16}O) with a relativistic mean-field description in an RRPA calculation and results obtained with the NL3 parametrization are compared to our experimental results [18,25] in Table III. For each nucleus the calculated energies are approximately 2 MeV above the experimental values. One of the improvements in the Ma *et al.* work is the inclusion of configurations coupling the empty state in the Dirac sea with occupied states in the Fermi sea ("ah coupling" in their notation) which had a substantial effect on the energy of the GMR [26] obtained from RRPA calculations and brought RRPA results into better agreement with time-dependent relativistic mean-field calculations for the GMR. This however "pushes" the GQR energies up substantially and the distributions calculated without ah coupling are in much better agreement with the experimental data.

The $E3$ strength is split into a lower component at $E_x \sim 12$ MeV, containing $\sim 8\%$ of the isoscalar $E3$ EWSR, probably a portion of the low energy octupole resonance-(LEOR), and the high energy octupole resonance (HEOR) centered at $E_x \sim (22.9+0.7-0.5)$ MeV containing $78+9-15\%$ of the isoscalar $E3$ EWSR. The $1\hbar\omega$ LEOR resonance [27] generally contains approximately 25% of the $E3$ EWSR, but lies mostly below the 10 MeV threshold of this experiment. Bertrand *et al.* [28] with 200 MeV proton scattering reported 18% of the $E3$ EWSR centered at 27 MeV while Yamagata *et al.* [29] using 100 MeV ^{3}He scattering reported 47% of the $E3$ EWSR centered at 26.5 MeV. Neither of these experiments did the small angle scattering necessary to distinguish $E1$ from $E3$ strength (at the time of these experi-

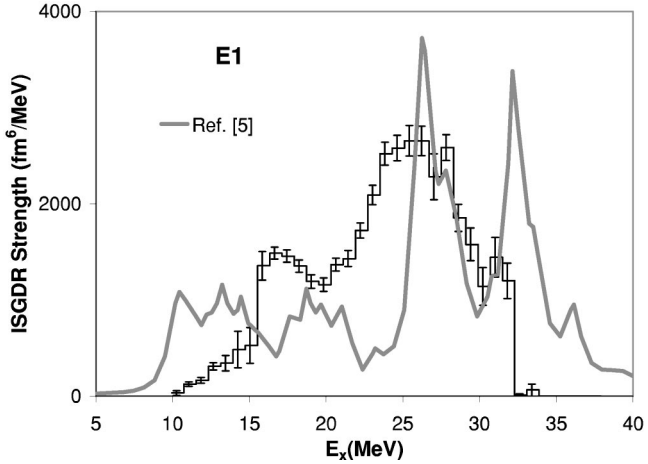

FIG. 6. The ISGDR strength function calculated by Colò *et al.* [5] is compared to the experimental strength function obtained from the data shown in Fig. 3.

TABLE III. ISGQR peak positions.

	Ma *et al.* [24] E_x (MeV)	Experiment E_x (MeV)
^{40}Ca	19.8	17.84 ± 0.43[a]
^{90}Zr	16.4	14.65 ± 0.20[b]
^{208}Pb	12.8	10.89 ± 0.30[c]

[a]Reference [25].
[b]This work.
[c]Reference [18].

ments, the ISGDR had not been observed in ^{90}Zr). As $E1$ and $E3$ angular distributions differ significantly only at small angles, it is likely that too high a continuum was used during the analysis of both of these experiments causing them to miss the strength around 21 MeV, so that the strength they attribute to the HEOR is actually a combination of the $E3$ and $E1$ strength in the region of 27 MeV.

V. CONCLUSIONS

Within errors, all of the $2\hbar\omega$ isoscalar $E0$ strength and most of the isoscalar $E1$, $E2$, and $3\hbar\omega$ $E3$ giant resonance strength was located in ^{90}Zr in the region $10 < E_x < 35$ MeV. Much of the $E0$ strength is concentrated in a Gaussian like peak centered around 16 MeV but the strength continues up to above $E_x = 25$ MeV resulting in a centroid of $(17.81 + 0.32 - 0.20)$ MeV. This is in agreement with the results of Ref. [3] which led to the conclusion that $K_{\mathrm{NM}} \sim 231$ MeV. A HF-RPA calculation by Hamamoto, Sagawa, Zhang [19] shows a similar tailing of the strength while an RRPA calculation by Piekarewicz [20] using the NLC parametrization ($K_{\mathrm{NM}} = 224$ MeV) gives a good representation of the shape of the distribution but lies a few hundred keV high. The ISGDR is seen to consist of two components, the upper component (presumably) being the compression mode [5,6]. Microscopic predictions with RPA-HF calculations [5] with the SGII ($K_{\mathrm{NM}} = 215$ MeV) interaction and relativistic calculations [20] for ^{208}Pb using the NLC parametrization ($K_{\mathrm{NM}} = 224$ MeV) show the compression mode peak higher than the experimental peak by 1–2 MeV, similar to ^{116}Sn, ^{144}Sm, and ^{208}Pb [18]. Whether this is a problem with the models or an experimental issue of missing strength is not clear.

ACKNOWLEDGMENTS

This work was supported in part by the U.S. Department of Energy under Grant No. DE-FG03-93ER40773 and by The Robert A. Welch Foundation.

[1] J. P. Blaizot, Phys. Rep. **64**, 171 (1980).
[2] S. Stringari, Phys. Lett. **108B**, 232 (1982).
[3] D. H. Youngblood, H. L. Clark, and Y.-W. Lui, Phys. Rev. Lett. **82**, 691 (1999).
[4] H. L. Clark, Y.-W. Lui, and D. H. Youngblood, Phys. Rev. C **63**, 031301(R) (2001).
[5] G. Colò, N. Van Giai, P. F. Bortignon, and M. R. Quaglia, Phys. Lett. B **485**, 362 (2000).
[6] D. Vretenar, A. Wandelt, and P. Ring, Phys. Lett. B **487**, 334 (2000).
[7] D. M. Pringle, W. N. Catford, J. S. Winfield, D. G. Lewis, N. A. Jelley, K. W. Allen, and J. H. Coupland, Nucl. Instrum. Methods Phys. Res. A **245**, 230 (1986).
[8] S. Kowalski and H. A. Enge (unpublished).
[9] D. H. Youngblood, Y.-W. Lui, and H. L. Clark, Phys. Rev. C **60**, 014304 (1999).
[10] Jon Patrick Oliver, M.S. thesis, Texas A&M University, 1996.
[11] K. van der Borg, M. N. Harakeh, and A. van der Woude, Nucl. Phys. **A365**, 243 (1981).
[12] H. L. Clark, Y.-W. Lui, and D. H. Youngblood, Nucl. Phys. **A687**, 80c (2000); in *Proceedings of the Seventh International Topical Conference on Giant Resonances, Osaka, Japan*, edited by M. Fujiwara, H. Ejiri, M. Nomachi, and T. Wakasa (12-15 June 2000).
[13] G. R. Satchler and Dao T. Khoa, Phys. Rev. C **55**, 285 (1997).
[14] M. Rhoades-Brown, M. H. Macfarlane, and S. C. Pieper, Phys. Rev. C **21**, 2417 (1980); M. H. Macfarlane and S. C. Pieper, Argonne National Laboratory Report No. ANL-76-11, 1978 (unpublished).
[15] D. H. Youngblood, Y.-W. Lui, and H. L. Clark, Phys. Rev. C **55**, 2811 (1997).
[16] M. N. Harakeh and A. E. L. Dieperink, Phys. Rev. C **23**, 2329 (1981).
[17] S. S. Dietrich and B. L. Berman, At. Data Nucl. Data Tables **38**, 199 (1988).
[18] D. H. Youngblood, Y.-W. Lui, H. L. Clark, B. John, Y. Tokimoto, and X. Chen, Phys. Rev. C **69**, 034315 (2004).
[19] I. Hamamoto, H. Sagawa, and X. Z. Zhang, Phys. Rev. C **56**, 3121 (1997).
[20] J. Piekarewicz, Phys. Rev. C **64**, 024307 (2001).
[21] M. Buenerd, C. Bonhomme, D. Lebrun, P. Martin, J. Chauvin, G. Duhamel, G. Perrin, and P. de Saintignon, Phys. Lett. **84B**, 305 (1979).
[22] D. H. Youngblood, P. Bogucki, J. D. Bronson, U. Garg, Y.-W. Lui, and C. M. Rozsa, Phys. Rev. C **23**, 1997 (1981).
[23] W. T. A. Borghols *et al.*, Nucl. Phys. **A504**, 231 (1989).
[24] Zhong-yu Ma, A. Wandelt, Nguyen Van Giai, D. Vretenar, P. Ring, and Li-gang Cao, Nucl. Phys. **A703**, 222 (2002).
[25] D. H. Youngblood, Y.-W. Lui, and H. L. Clark, Phys. Rev. C **63**, 067301 (2001).
[26] P. Ring, Zhong-yu Ma, Nguyen Van Giai, D. Vretenar, A. Wandelt, and Li-gang Cao, Nucl. Phys. **A694**, 249 (2001).
[27] A. van der Woude, Int. Rev. Nucl. Phys. **7**, 100 (1991).
[28] F. E. Bertrand, E. E. Gross, D. J. Horen, J. R. Wu, J. Tinsley, D. K. McDaniels, L. W. Swenson, and R. Liljestrand, Phys. Lett. **103B**, 326 (1981).
[29] T. Yamagata, S. Kishimoto, K. Yuasa, K. Iwamoto, B. Saeki, M. Tanaka, T. Fukuda, I. Miura, M. Inoue, and H. Ogata, Phys. Rev. C **23**, 937 (1981).